Role of hydrogen in the electronic properties of CaFeAsH-based superconductors

Y. N. Huang,[1,2,3] D. Y. Liu,[1] L. J. Zou,[1,2,*] and W. E. Pickett[3,†]

[1]*Key Laboratory of Materials Physics, Institute of Solid State Physics, Chinese Academy of Sciences, P. O. Box 1129, Hefei 230031, China*

[2]*University of Science and Technology of China, Hefei, Anhui 230026, China*

[3]*Department of Physics, University of California Davis, Davis, California 95616, USA*

(Received 26 February 2016; revised manuscript received 17 April 2016; published 23 May 2016; corrected 4 August 2017)

The electronic and magnetic properties of the hydride superconductor CaFeAsH, which superconducts up to 47 K when electron doped with La, and the isovalent alloy system $CaFeAsH_{1-x}F_x$ are investigated using density functional based methods. The $\vec{Q} = (\pi,\pi,0)$ peak of the nesting function $\xi(\vec{q})$ is found to be extremely strong and sharp, and the additional structure in $\xi(\vec{q})$ associated with the near-circular Fermi surfaces (FSs) that may impact low energy excitations is quantified. The unusual band introduced by H, which shows strong dispersion perpendicular to the FeAs layers, is shown to be connected to a peculiar van Hove singularity just below the Fermi level. This band provides a three-dimensional electron ellipsoid Fermi surface not present in other Fe-based superconducting materials nor in CaFeAsF. Electron doping by 25% La or Co has a minor effect on this ellipsoid Fermi surface, but suppresses FS nesting strongly, consistent with the viewpoint that eliminating strong nesting and the associated magnetic order allows high T_c superconductivity to emerge. Various aspects of the isovalent alloy system $CaFeAsH_{1-x}F_x$ and means of electron doping are discussed in terms of influence of incipient bands.

DOI: 10.1103/PhysRevB.93.195148

I. INTRODUCTION

Identifying and studying similar materials that display very different behavior has been an active approach to understanding the origin of high temperature (T_c) superconducting Fe-based pnictides and chalcogenides, and is expected to promote the quest for new and possibly higher T_c superconductors. In this class of materials, elemental substitution can be done in an isovalent manner to provide (seemingly) minor changes, while aliovalent substitution supplies either electron or hole carriers to the Fe 3*d* bands [1–5]. Each method can provide insight not otherwise obtainable.

While there are now several classes of Fe-based superconductors, and most are well studied, the recently synthesized CaFeAsH [6–9], with its H^- anion [10] in the blocking layer, adds a new dimension to the phenomenon. Hosono *et al.* [10] showed that hydrogen in this material can form a solid solution in any ratio with F^-, making $CaFeAsF_{1-x}H_x$ an isovalent, isostructural system in which specific differences can be varied continuously. Though Muraba *et al.* [7] have emphasized some important differences from the oxide analogs in the electronic structure, the differences arising from H versus F have not been studied thoroughly. Such isovalent sister compounds provide means to evaluate the effects of specific, seemingly small differences, such has been exploited in the LiFeAs, NaFeAs, and MgFeGe compounds, which likewise are isoelectronic and isostructural with extremely similar band structures [11–14], but differing properties. In fact, MgFeGe is not superconducting at all. Though nonsuperconducting at ambient pressure, both CaFeAsH and CaFeAsF display pressure-driven superconductivity with T_c up to 25–28 K at the superconducting onset at 3–5 GPa, beyond which T_c decreases with additional pressure [15].

Impressively, indirect electron doping by La on the Ca site of CaFeAsH produces superconductivity [6] with $T_c^{\max} = 47$ K, in the regime of the rare earth 1111 compounds with the highest T_c's (up to 56 K). This high T_c can be contrasted with "direct" electron doping by Co substitution of Fe, which attains [7] only $T_c^{\max} = 23$ K. Also noteworthy is that in both cases there is no superconducting dome—the "onset T_c" (some samples are evidently not homogeneous) is almost constant [6,16] from the appearance of superconductivity at a doping level at $x = 0.07$–0.08 to the maximum doping studied $x = 0.3$–0.4.

There are strong parallels to another two-dimensional (2D) electron-doped system A_xMNCl, where $M = Zr$ (respectively Hf), A is an alkali metal, with a T_c of 15 K (respectively, 26 K). In these two compounds T_c is independent of doping level [17] except at the low end, at the onset of superconduction where T_c is somewhat higher. This indifference of T_c to the evolving electronic structure has been discussed [18], and this same indifference in CaFeAsH raises important questions, since there is a great deal of evidence in other Fe-based superconductors that properties including T_c are sensitive to small changes in electronic structure. There are differences in T_c and other properties with chemical variation on the H/F site, in addition to the doping differences, that so far have no explanation.

Incorporation of H as an anion in the blocking layer and the realization of the superconductivity as high as 47 K invites certain questions. First, within the same 1111 phase, why does T_c increase so much with La doping after $(LaO)^+$ layers are replaced by isovalent $(CaH)^+$ layers? Second, in comparison with CaFeAsF, what is the role of H in stabilizing such a high T_c? A third question is why the maximal superconducting critical temperatures in La-doped and Co-doped CaFeAsH samples (both electron doped) are so different? These are the sort of issues we try to shed light on.

Using methods similar to those we use (see below), Muraba *et al.* [7] and Wang and collaborators [19] have identified the main differences in the band structures of CaFeAsH and

*zou@theory.issp.ac.cn

†wepickett@ucdavis.edu

CaFeAsF: the former has an additional Fermi surface arising from a band that is displaced from its position in the F compound and in other 1111 compounds. While it is in all cases a primarily Fe $3d$ band, the H $1s$ states are less strongly bound than the F $2p$ states and evidently provide a propitious pathway for Fe-As-H-As-Fe hopping from FeAs layer to FeAs layer. Fermi surface nesting was discussed but the difference between the H and F compounds was not quantified.

These differences, and the electronic structure to be analyzed here, call to mind the recent discussion on the possible influence of incipient bands in Fe-based superconductors. Incipient bands are those that do not actually cross the Fermi energy (E_F) and thus do not have an associated Fermi surface, but are near enough to the Fermi level (within a pairing cutoff energy) to contribute to pairing and superconductivity. Chen *et al.* [20], who provide an excellent overview of the discussion, conclude that incipient bands may indeed play a role in pairing in LiFeAs and in FeSe monolayers on $SrTiO_3$ substrates. The difference in the electronic structures at or near the Fermi level, and the associated (magnetic) fluctuations, in these H and F compounds must account for their differing properties, and the incipient band viewpoint may be a useful one to consider.

In this paper first-principles methods, described in Sec. II, are applied to study the electronic structures and magnetic ground states of CaFeAsH and CaFeAsF, and the nonmagnetic and superconducting electron-doped phases $Ca_{0.75}La_{0.25}FeAsH$ and $CaFe_{0.75}Co_{0.25}AsH$. Section III contains the main results. It is confirmed that CaFeAsH has, in addition to the nearly circular, 2D electron and hole cylinders expected of an Fe 1111 compound, a strongly k_z-dispersive band crossing the Fermi level (E_F) that leads to a three-dimensional (3D) ellipsoidal Fermi pocket, whose implications we explore. A specific feature that we quantify is extremely sharp $\vec{Q} = (\pi,\pi,0)$ nesting (as usual, in units of in-plane lattice constant $a = 1$). Several other differences between the H and F compounds are analyzed, including nesting away from the nesting peak at $\vec{Q}$ that may impact low energy properties. A short summary is provided in Sec. IV.

II. STRUCTURE AND METHODS

A. Crystal structure

The crystal symmetry across the $CaFeAsF_{1-x}H_x$ system is tetragonal $P4/nmm$, comprised of alternating Ca_2H_2 and Fe_2As_2 layers as in Fe-based 1111 compounds [21]. The hydride and fluoride ions have closed shell, negatively charged ionic configurations with not greatly differing anionic radius, allowing the successful synthesis of all solid solutions [9]. As mentioned, CaFeAsH displays differences compared to CaFeAsF [22,23], which is part of the motivation for this study.

The experimental lattice parameters are used in the calculations. In the $P4/nmm$ phase above the magnetic ordering temperature, for CaFeAsH [7] $a_t = 3.879$ Å, $c_t = 8.26$ Å. For CaFeAsF [24] the lattice parameter $a = 3.878$ Å is nearly identical, while $c = 8.593$ Å. Thus the larger F ion, confirmed by charge density plots (not shown), enlarges the structure only along the c axis. For CaFeAsH in the magnetically ordered $Cmma$ phase, a=5.457 Å=1.407a_t, $b = 5.492$ Å = 1.416a_t, and $c = 8.21$ Å = 0.994c_t. For $Ca_{0.75}La_{0.25}FeAsH$ and $CaFe_{0.75}Co_{0.25}AsH$ in the tetragonal phase, the unit cell size is $2a \times b \times c$, $a = 3.883$ Å = 1.001a_t, $c = 8.20$ Å = 0.993c_t [16].

It will be useful to be aware of the distances between the As plane and the anion plane. For CaFeAsH, d(As-H) = 2.71 Å; for CaFeAsF, d(As-F) = 2.89 Å. For comparison, in LaFeAsO, the separation is d(As-O) = 3.05 Å. These differences have the potential to affect k_z dispersion, that is, the three-dimensional character, which is an issue that we study.

B. Calculational methods

The full-potential linearized augmented plane wave Wien2K package [25] has been used for the electronic structure calculations. We use the Perdew, Burke, and Ernzerhof [26] version of the generalized gradient approximation (GGA) to the exchange-correlation functional within density functional theory. The sphere radii for Ca, H, Fe, As, F, La, and Co are taken as 2.50, 1.40, 2.39, 2.12, 2.20, 2.50, and 2.38 bohrs, respectively. The basis set cut-off parameter $R_{mt}K_{\max} = 7.0$ was found to be sufficient. The number of $\vec{k}$ points was typically 3000 for the tetragonal unit cell.

The magnetic order commonly observed in these Fe-based two-dimensional (2D) materials leads us to study the relative energetics of ordered phases. The primitive tetragonal cell contains two Fe sites, due to the tetrahedral coordination with As ions. The Fe sublattice is square, oriented at 45° with respect to the conventional cell. One possible magnetic order is the Néel type, in which each Fe on its square sublattice is anti-aligned with its four neighbors; this is $\vec{q} = 0$ AFM order (NAFM). Stripe AFM (SAFM) order corresponds to each Fe atom being antiparallel to its neighbors along the $\vec{a}$ and $\vec{b}$ axes, which are second Fe neighbors. SAFM corresponds to $\vec{Q} = (\pi,\pi,0)$ order, and typically destroys much of the Fermi surface. The SAFM unit cell size is doubled to $\sqrt{2} \times \sqrt{2} \times 1$.

III. ANALYSIS AND DISCUSSION

A. Nonmagnetic phase: A new band

Figure 1 displays the band structure and Fermi surfaces of CaFeAsH in the nonmagnetic phase. There are two cylindrical hole bands around the $\Gamma = (0,0,0)$ point and two cylindrical

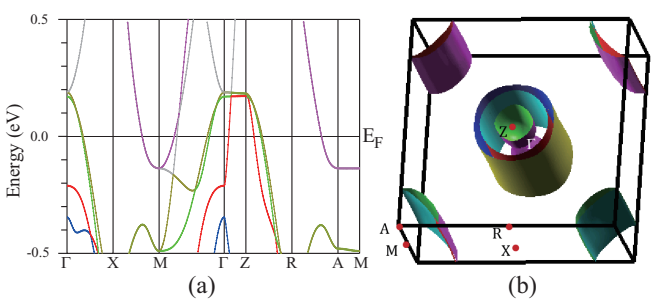

FIG. 1. The (a) electronic band structure and (b) Fermi surface is of CaFeAsH in its nonmagnetic phase. In (b) the Γ point in the center of the figure.

electron bands crossing E_F near the $M = (\pi,\pi,0)$ point, consistent with those presented by Muraba *et al.* [6]. This band structure is similar to that of the LaFeAsO 1111-type compounds, except for an additional central Fermi surface around the Z point of the zone. The apparent nesting, which we quantify below, implies that CaFeAsH has a tendency toward the SAFM order phase observed and obtained computationally in other 1111 compounds.

The distinctive feature of these bands is the existence of one band along the Γ-Z direction that shows not only k_z dispersion but a surprisingly large velocity along k_z. This band gives rise to an additional, ellipsoidal in shape, hole Fermi surface surrounding the Z point of the zone. Bands near E_F, including the unusual one, have strongly Fe d_{xy} and d_{xz},d_{yz} character, with small As $4p$ character. This new Fermi surface has similarities to one in a magnetically ordered phase of LaFePO that is different from the corresponding Fermi surface of LaFeAsO in the same magnetic structure [27]. The k_z dispersion is however much less dramatic in LaFePO than in CaFeAsH.

B. Electronic structure: H versus F

Muraba *et al.* [8] have shown that the F $2p$ and H $1s$ bands lie well below the Fermi level and are filled, so each is a negatively charged (-1) ion. The densities of states (DOS) in Fig. 2(a) demonstrate that the F states are 2 eV more strongly bound than the H $1s$ states. Figure 2(a), right panel, also shows the corresponding projected density of states (PDOS) near E_F.

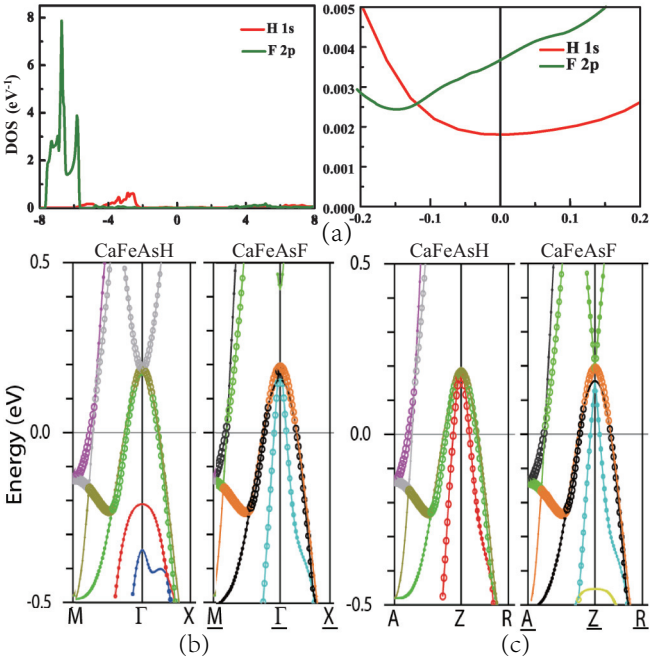

FIG. 2. (a) Left panel: The PDOS of H $1s$ orbital in CaFeAsH and F $2p$ orbitals in CaFeAsF, revealing the substantially larger binding energy of the F states. (a) Right panel: An enlargment of the PDOS around the Fermi energy. (b) and (c) The band structures of both compounds, along the paths (b) M-Γ-X and (c) A-Z-R at the top of the zone. Paths with underlined letters are for CaFeAsF. The thickness of the bands shows the relative amount of Fe $d_{xz} + d_{yz}$ character.

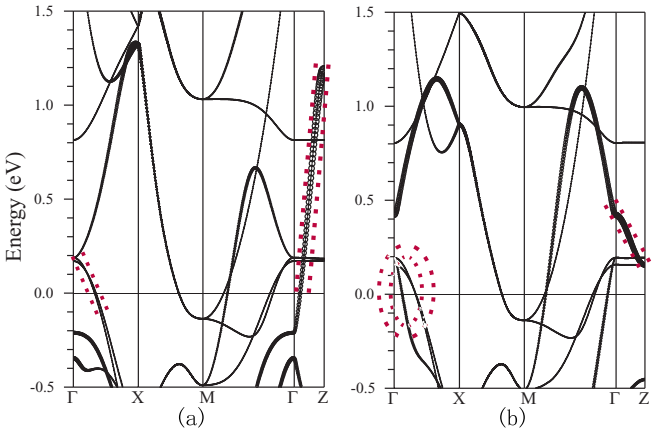

FIG. 3. The contribution of the arsenic atomic $4p_z$ orbital to (a) CaFeAsH and (b) CaFeAsF bands near E_F. The dashed red lined regions emphasize areas of differences in bands along the Γ-X and Γ-Z directions, see text.

These curves likely reflect not the atomic states but the tails of neighboring atomic orbitals that extend into the H and F atomic regions. The point is that these are states near E_F and their distributions and hybridization are significantly different. It is this and related differences that we pursue in this subsection.

The Fermi surface differences noted in Sec. III A do not convey the extent of the differences in electronic structure caused by H versus F. Figures 2(b) and 2(c) show the band dispersions, weighted by Fe $d_{xz} + d_{yz}$ character, in the M-Γ-X and the zone top A-Z-R paths. In CaFeAsF, there are three holelike bands centered around the Γ-Z line, and the bands display no k_z dispersion. For CaFeAsH, however, two holelike bands cross E_F along the M-Γ-X path while three holelike bands crosses the E_F along the A-Z-R path. The difference is that in the H compound, a band at Γ 0.2 eV below E_F in CaFeAsF lies 0.2 eV above E_F at Z.

Figure 3 shows the bands along the most relevant symmetry lines, weighted this time by the amount of As $4p_z$ character. Most prominently, in CaFeAsH, a band is essentially linear from Γ to Z—very large k_z dispersion—over an energy span of 1.5 eV. The velocity is $\hbar v_F = 3.8$ eV Å, or $v_F = 5.9 \times 10^8$ cm/s. The bonding path that enables this large interlayer hopping is Fe-As-H-As-Fe, identified previously [6,19]. Visible in Fig. 3(b) is that the corresponding band in CaFeAsF has a factor of ∼7 less dispersion, and in the opposite direction. Also, it lies entirely above E_F so it does not affect the FS.

A plot through the zone Z-Γ-Z would indicate this dispersive band in CaFeAsH to be Dirac-like at -0.2 eV, except that it (necessarily by symmetry) becomes quadratic extremely close to Γ. However, this band disperses downward in both directions in plane, so the point at Γ is a van Hove singularity (vHs) with two normal negative masses $m_x = m_y$ and an extremely small positive mass along the k_z direction, whereupon the band quickly becomes linear (massless). Lying 0.2 eV below E_F this vHs has no influence on low energy properties (including, we expect, superconductivity) but it reflects a highly unusual influence of H in this structure. A very similar linear valence band has been found in the $CoAs_3$ class of skutterudites where it has been analyzed in detail [28,29] and

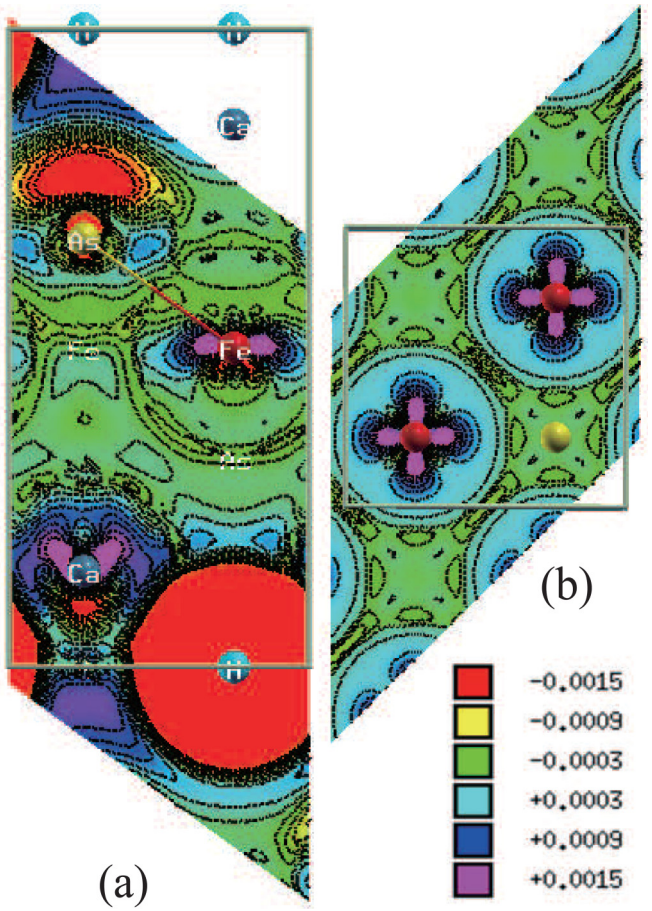

FIG. 4. Contour plots of the density difference ρ(CaFeAsH)-ρ(CaFeAsF). (a) A (110) plane containing the Fe-As zigzag chain (and also the Ca and H/F sites). (b) (001) plane through Fe sites. The large red region in (a) denotes where contours have been cut off due to the large and meaningless difference of the H and F densities.

found to arise from a cluster orbital of As p states surrounding the open hole in this lattice.

There is an additional H versus F difference evident in Fig. 3(b). Of the pair of hole bands extending from Γ, the Fermi surfaces are circular and nearly identical in CaFeAsH, while the values of k_F in CaFeAsF differ. The cylinders include different numbers of holes, and the larger number of holes in CaFeAsH are balanced by the electrons in the ellipsoid that does not exist in CaFeAsF. This difference also affects the nesting function which can be seen in plots from a careful study that we present below.

C. Fe layer charge: H versus F

Due to the focus of attention in Fe-based pnictides and chalcogenides on Fe orbital occupations and how they relate to properties, we have calculated the difference density ρ(CaFeAsH)-ρ(CaFeAsF), with both calculated at the lattice constant of the former compound. Figure 4 shows contour plots of this difference density in two planes: a (110) plane containing a FeAs zigzag chain, and a (001) plane through the Fe sites. Positive values designate regions where H attracts charge relative to F.

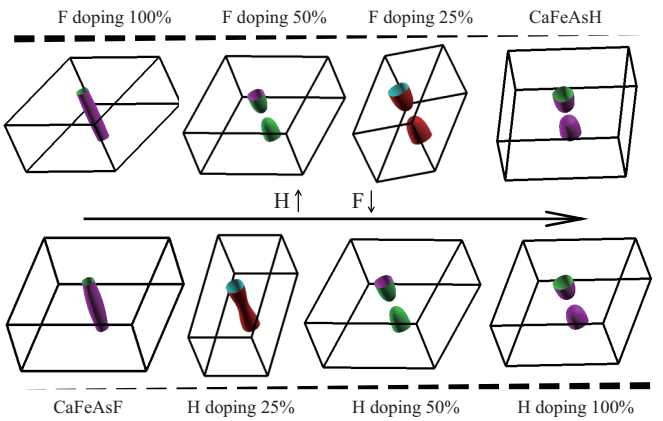

FIG. 5. Plots of the Fermi surfaces at Γ for the isovalent alloy series CaFeAs(H,F). Labels indicate the relative fractions of H and F. Upper row: F doping at the CaFeAsH structural parameters. Lower row: H doping at the CaFeAsF structural parameters.

In the horizontal plane containing Fe sites, Fig. 4(b), H is seen to increase charge in the in-plane orbitals while there is a slight decrease in density in the interstitial region in both planes. In the Fe-As chain direction, Fig. 4(a), the increase in occupation of the Fe in-plane orbitals is again evident. What is more evident is the larger change on As, with charge "transferred" to the p_x, p_y orbitals at the expense of the p_z orbital. In addition, there are changes on the Ca ion of the same size as on Fe. Density is slightly decreased in the interstitial region.

These differences can be quantified by subtracting the orbital occupations, CaFeAsH minus CaFeAsF, within the atomic spheres. In units of 10^{-3}, the differences for Fe are d_{z^2}, 2.5; d_{xy}, 7.6; $d_{x^2-y^2}$, 3.5; $d_{xz} = d_{yz}$, −0.6. The net change for Fe is $+12.4 \times 10^{-3}$ electrons. For As, the analogous changes are p_x, p_y, 5.9; p_z, −9.9, for a small net change of $+1.9 \times 10^{-3}$ electrons. Thus H induces ∼0.015 electrons into the Fe + As spheres compared to F, with the decrease occurring in the interstitial region or in the Ca(H,F) region.

D. Study of $H_{1-x}F_x$ substitution

To determine whether the Fermi surface differences (and band structure differences) are affected by the different lattice parameters, we have replaced H by F in CaFeAsH and replaced F by H in CaFeAsF, each with its own value of the c lattice parameter [7,24]. The differences in the 3D ellipsoid FS sheet are shown in Fig. 5, replacing H by $H_{1-x}F_x$ in CaFeAsH, for $x = 1, \frac{1}{2}, \frac{1}{4}, 0$, and replacing F by H_yF_{1-y} in CaFeAsF ($y = 0, \frac{1}{4}, \frac{1}{2}, 1$). The effect of c lattice constant is very small; note that in each of the cases $x = 0, \frac{1}{2}$, and 1 the surfaces are very similar, with the pinching off of the cylinder occurring around 35%–40% H. Evidently the difference is a chemical bonding one that is much more important than intersublayer separations.

E. Fermi surface nesting

Fermi surface nesting has played a central role in theories of the Fe-based superconductors, on the one hand accounting for the observed AFM phases in several undoped compounds and

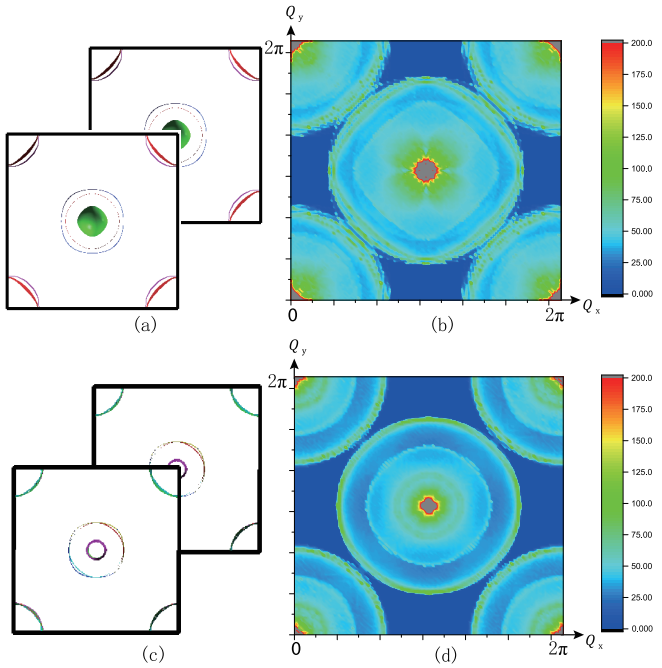

FIG. 6. Left column: Top view of Fermi surface sheets of nonmagnetic (a) CaFeAsH and (c) CaFeAsF. The FS contours are overlaid by a copy displaced by $\mathbf{Q} = (\pi,\pi,0)$. The close overlap of hole and electron pockets indicates strong Fermi surface nesting. Right column: The $\mathbf{q}$-space plot of the nesting function $\xi(\mathbf{q})$ of (b) CaFeAsH and (d) CaFeAsF as described in the text. The plot covers the entire zone, with the plot centered at $\mathbf{Q} = (\pi,\pi,0)$; Γ points lie at the corners. The structures are described in the text.

on the other as promoting short-range AFM fluctuations that may provide the superconducting pairing mechanism. Both of these aspects focus on the susceptibility peak near $\vec{Q} = (\pi,\pi,0)$, as discussed for Fe pnictides earlier [30,31]. However, nesting processes, i.e., those which scatter from Fermi surface to Fermi surface, dominate all low energy processes, and it may be important to understand such process throughout the Brillouin zone.

With an eye first toward the magnetic instability in CaFeAsH and CaFeAsF and the wave vector dependence of magnetic fluctuations in the (high temperature) tetragonal structure, we analyze the Fermi surface topology in the nonmagnetic phase. The top view of Fermi surface sheets is shown in Figs. 6(a) and 6(c), with a copy displaced by $\vec{Q}$. The cylindrical, nearly circular, FS sheets at M, and two of the three at Γ, reflect the 2D character of these Fermi surfaces. As mentioned, a substantial degree of $\vec{Q}$ nesting is evident, which we proceed to quantify below. While the circular FSs around Γ in CaFeAsH essentially coincide, in the F compound the inner sheet is much smaller, arising from the difference in band structures discussed above.

1. Formalism

A quantitative measure of nesting is provided by the Fermi surface nesting function $\xi(\vec{q})$, which measures the phase space for scattering through wave vector $\vec{q}$ from $\vec{k}$ on the FS to $\vec{k}+\vec{q}$ also on the FS. This function is given by

$$\xi_{\mathbf{q}} = \sum_k \delta(\varepsilon_{\vec{k}} - \varepsilon_F)\delta(\varepsilon_{\vec{k}+\vec{q}} - \varepsilon_F) = \frac{\Omega_c}{(2\pi)^3}\int_{\updownarrow} \frac{d\mathcal{L}_{\vec{k}}(\varepsilon_F)}{|\vec{v}_k \times \vec{v}_{k+q}|}, \quad (1)$$

here Ω_c is the cell volume and $\vec{v}_k = \nabla_k \varepsilon_k$ is the electron velocity ($\hbar = 1$). The latter expression, after the volume integral with two δ-function restrictions, gives a geometrical interpretation: it is the integral over the line of intersection $\mathcal{L}_{\mathbf{k}}(\varepsilon_F)$ of the undisplaced FS and a copy of the FS displaced by $\vec{q}$, weighted by the inverse of the cross product of the two velocities. Large contributions arise from regions of parallel or antiparallel velocities, i.e., FS nesting where the velocity cross product becomes small. Contributions are enhanced by small velocities, although that is not an issue with these cylindrical FSs that arise in these compounds, with near constant Fermi velocities around the FSs. $\xi(\vec{q})$ has a trivial q^{-1} divergence at $q \to 0$ that is countered by vanishing matrix elements in physical properties involving such long wavelength momentum transfers.

Fermi surface instabilities are more often analyzed in terms of the electronic susceptibility, which is the relevant response function,

$$\chi_0(\mathbf{q}) = \frac{1}{N}\sum_{k,m,n} |M_{kn,k+qm}|^2 \frac{f(\varepsilon_{\vec{k}+\vec{q},m}) - f(\varepsilon_{\vec{k},n})}{\varepsilon_{\vec{k}+\vec{q},m} - \varepsilon_{\vec{k},n} + i\eta}, \quad (2)$$

where $M_{km,k'n}$ is a matrix element of $\exp(i\vec{q}\cdot\vec{r})$ between Bloch functions. Though matrix elements often are important, evaluations without matrix elements, corresponding to the "generalized susceptibility," are much more common. Peaks in the real part of $\chi_0(\vec{q})$ provide the positions of potential wave vector $\vec{q}$ instabilities. Structure in $\chi_0(\vec{q})$ arises from Fermi surface nesting as well as from other near-E_F structure in the band structure, viz. the virtual bands that will be discussed below.

Instabilities in the metallic phase, often phrased as instabilities of the Fermi surface, are characterized in terms of peaks in the real part of the electronic susceptibility. The nesting function defined above has its own separate importance. To first (linear) order in small ω the connection to the imaginary part χ_0'' of the dynamical susceptibility (here matrix elements are set to unity) is

$$\chi_0''(\vec{q},\omega) = \pi\omega\xi(\vec{q}) + O(\omega^2). \quad (3)$$

Thus low energy dissipative processes occur where there is strong weight in $\xi(\vec{q})$, in addition to the Drude interband absorption at small $|\vec{q}|$.

2. Discussion of nesting

The behavior of $\xi(\vec{q})$ in both compounds is dominated by the very strong peak precisely at $\vec{Q}$. In several Fe-based pnictides a maximum at this wave vector also shows up in $\chi(\vec{q},\omega = 0)$ but probably not with nesting as perfect as in this F compound, where Fig. 6(c) illustrated the perfect nesting of the outer electron and hole surfaces in CaFeAsF. The nesting is not as perfect for CaFeAsH, but there are two surfaces of each type of carrier that nest. Note that in the dark regions

of these plots there is zero nesting, there are no low energy excitations in these regions, a result of the relatively small Fermi surfaces. Of interest, of course, is that the near perfect nesting at $\vec{Q}$ indicates a strong tendency for AFM order, and that (electron) doping will degrade the nesting and thereby diminish the tendency for magnetic ordering.

Additional structure can be seen in $\xi(\vec{q})$ that is difficult to see in the susceptibility. In 2D, a circular FS of radius k_F gives rise to a characteristic divergence [32,33] $1/\sqrt{2k_F - q}$ as $q = |\vec{q}|$ approaches $2k_F$, then vanishes abruptly for $q > 2k_F$, where transitions are no longer available. The essentially identical in size circular FSs of CaFeAsF give rise to this characteristic circular peak at radius of $2k_F$ around $\vec{q} = 0$ and almost identically around $\vec{q} = \vec{Q}$, easily visible in the figure. Since phonons acquire renormalization from small (nearly zero) energy processes, $\xi(\vec{q})$ suggests strong phonon renormalization at the nesting wave vector and smaller but definite Kohn anomalies on the $q \approx 2k_F$ and $|\vec{q} - \vec{Q}| \approx 2k_F$ circular ridges. Spin waves should acquire renormalization in the same regions, for the same reasons.

Figure 6(b) provides the nesting function for CaFeAsH in comparison to that of CaFeAsF in Fig. 6(d). In the H compound, the noncircular nature of the ridges of $\xi(\vec{q})$ reflect the not-quite-circular Fermi surfaces. In addition, there is additional structure near the peaks at Γ and $\vec{Q}$ that arise from the ellipsoidal Fermi surface. Taking the broader picture, however, there is little quantitative difference between the nesting functions of these isoelectronic compounds.

F. Antiferromagnetic phases

Here we discuss magnetic energies and the basic features of the electronic structure of the SAFM phase in undoped CaFeAsH, and draw some parallels with related pnictides. The types of AFM order that are studied are described in Sec. II B, some of which require a $\sqrt{2} \times \sqrt{2} \times 1$ supercell (there are two Fe sites within the primitive cell). The energies of four of the simplest magnetic configurations relative to the nonmagnetic phase are presented in Table I, where the Fe atomic sphere moments are also provided. It has been much discussed that Fe moments are overestimated by DFT methods [27,34,35], so magnetic energies will also be exaggerated, however relative orderings may still be meaningful. These relative energies are in almost the same order as in the related compound $CaFeAs_2$, but differ somewhat in magnitude [36,37], reflecting some sensitivity to the Fe-As structure or to the makeup of the blocking layer.

TABLE I. Total energy difference for CaFeAsH of five magnetic phases including nonmagnetic (NM), ferromagnetic (FM), Néel AFM (NAFM), striped AFM (SAFM), and bi-striped AFM (BSAFM). The reference is the energy of the NM phase ($\Delta E = E_{(A)FM} - E_{NM}$). The corresponding magnetic moment in the Fe sphere is given.

Magnetic structure	NM	FM	NAFM	SAFM	BSAFM
(a) Relative energy (meV)	0	−83	−119	−282	−163
(b) Fe moment (μ_B)	0	0.63	1.92	1.92	1.22

For FM alignment the moment is much smaller and the energy less favorable than for the AFM alignments. The smaller moments account qualitatively for the FM phase being less favorable. The SAFM state is most favorable by a large margin, 120 meV/Fe lower than the BSAFM phase. This lowest energy holds in spite of the SAFM phase having the same Fe spin moment of 1.92 μ_B as does the NAFM case. The differences in Fe moments in the various phases is evidence that the magnetism has substantial itinerant character. For itinerant magnets the energy gain for magnetism is $Im^2/4$, where I is the Hund's exchange coupling (also called Stoner I) and m is the moment. This behavior is not observed, arising possibly from nonlinear effects but also that the moment may not be of the simplest itinerant type.

For comparison, the SAFM moment of Fe is 2.18 μ_B in CaFeAsF, 13% higher than in CaFeAsH. Thus the differences in electronic structure discussed above significantly affect the magnetic predictions in these compounds. In CaFeAsF, the reported experimental moment is 0.49 μ_B [23], less than 25% of the calculated value. This discrepancy follows the known substantial overestimate of the moment in these Fe-based materials by DFT calculations. To our knowledge, no experimental moment has been reported for CaFeAsH, so it is unclear whether the differences in band structure between the H and F compounds show up experimentally.

Figure 7 shows the CaFeAsH SAFM band structure, Fermi surfaces, and projected Fe DOS. The magnetic ordering results in an orthorhombic cell, with a very low Fermi level density of states. The bands near E_F at Γ and M have been mixed and gapped by the SAFM order, so the cylindrical FSs

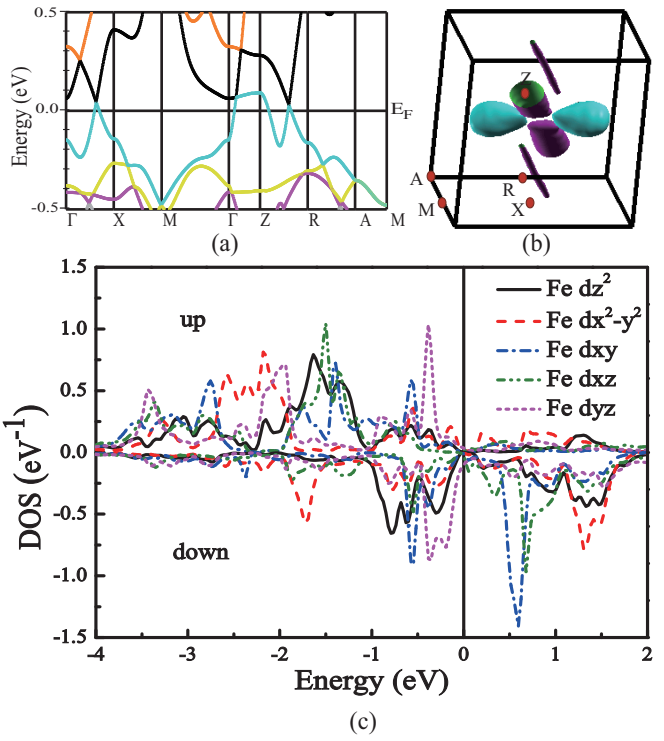

FIG. 7. For CaFeAsH with SAFM order: (a) Electronic band structure, (b) density of states, and (c) projected DOS for the Fe atom. Note the small DOS at the Fermi energy (zero of energy).

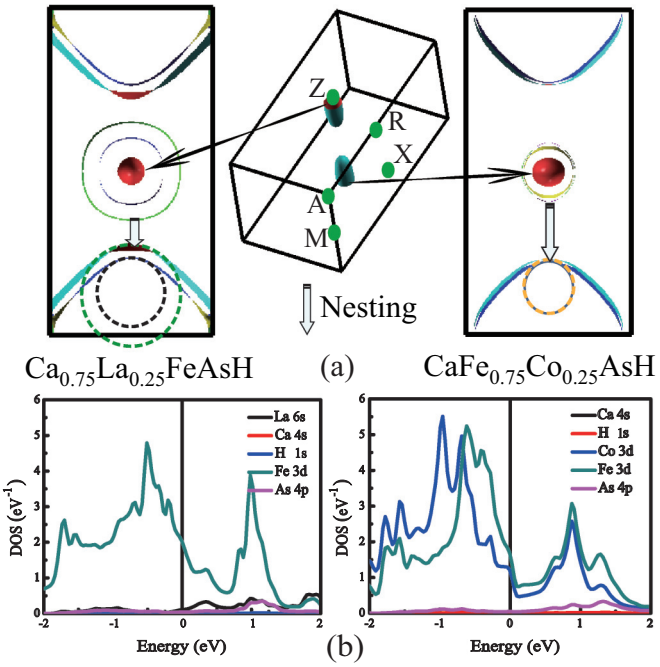

FIG. 8. (a) The Fermi surfaces and qualitative nesting features of $Ca_{0.75}La_{0.25}FeAsH$ and $CaFe_{0.75}Co_{0.25}AsH$, with electron doping in each case but indirect versus direct respectively. (b) Density of states (DOS) of each atom in $Ca_{0.75}La_{0.25}FeAsH$ (where only Fe is significant) and $CaFe_{0.75}Co_{0.25}AsH$, where Co can be compared with Fe.

have vanished, reflecting the massive electronic reconstruction driven by the nesting. The few remaining bands crossing E_F have high velocity.

The resulting electronic structure has noteworthy aspects. The majority states are filled (d^5). The minority states seem at first sight to have an expected e_g-t_{2g} splitting, however it is more complex than that. Evidently the SAFM order affects substantially the Fe configuration, based on the loss of tetrahedral symmetry due to magnetic reconstruction of the electronic bonding. There are substantial peaks of minority $d_{x^2-y^2}$ states both at -2 and $+1.5$ eV. The main d_{xy} peak is above E_F but a noticeable fraction lies below E_F. d_{xz} is mostly above E_F; d_{yz} is entirely below E_F. The magnetic order thus has a considerable effect on the orbital occupations and thereby the electronic structure.

G. La and Co doping phase

Both La and Co provide electronic doping, however Co introduces changes directly into the Fe layer while La simply donates electrons. Here we analyze the differences in electronic structure between indirect (La doping) and direct (Co doping) [6,7], to identify aspects that may correlate with the question of why $T_c^{\max}$ is a factor of 2 different in the two cases. We present results for the same 25% electron doping of the DOS and different Fermi surfaces of $Ca_{0.75}La_{0.25}FeAsH$ and $CaFe_{0.75}Co_{0.25}AsH$ in Fig. 8(a). The electron surfaces of course grow in size while hole surfaces decrease, and with substantial changes. We note that the onset T_c in the La-doped case remains around 47 K from $x = 0.08$ (metallization) to $x = 0.30$, the highest doping level reported. This makes our 25% case representative. The data indicate an unusual insensitivity to doping level, unlike the more common superconducting dome behavior with doping. It may however be possible that there is mesoscopic chemical phase separation in these sample such that the onset T_c represents the value of a single phase. For the homogeneous phases that we are modeling, there are substantial changes with doping.

The projected DOS curves of Fig. 8(b) reflect large differences. For La doping the Fe DOS hardly changes, with E_F increasing rigid-band like. The band filling of course is the same for Co doping. The Co $3d$ DOS differs from that of Fe, however, with the main peak lying 0.5 eV lower (higher binding energy), with the result that the contribution to $N(E_F)$ is substantially smaller. For this case E_F lies right at the top of a band, where $N(E)$ drops discontinuously. The H contribution at E_F is very small in both cases. The value of $N(E_F)$ is similar in the two cases, but disorder broadening may lower the value in the Co-doped case due to the step edge in $N(E)$.

The 3D ellipsoid pocket remains in each of these cases. Because the velocity along k_z is large, the extent of the ellipsoid along k_z does not increase much, being larger around the waist and larger in the Co doping case. The nesting of electron and hole FSs is severely degraded by 25% doping, a change that is conventionally associated with the destruction of spin density wave order that enables superconductivity to emerge. Although Cooper pairing due to short-range AFM fluctuations that are encouraged by nesting provides the most common explanation for superconductivity in Fe pnictides, there is no longer great interest in details of degraded nesting and we do not provide $\xi(\vec{q})$ for the doped materials. Figure 8(a) provides some indication of where some nesting remains, by repeating the electron FS cylinders displaced by the most evident displacement. The nesting lies at a larger displacement for Co doping and displays weaker nesting (the corresponding curvatures of the FSs differ more). Such differences might contribute to the factor of 2 difference in T_c, but the theory is not sufficiently established to pursue this point.

IV. SUMMARY

Density functional based methods have been applied to assess various aspects of the effect of Ca and H, versus La and O, on the underlying electronic structures of these 1111 compounds. Second, the differences in electron doping, by La for Ca or by Co for Fe, have been modeled and analyzed. The isovalent system CaFeAs(H,F) has also been studied. The key feature introduced by H is an unusual band dispersing along k_z, as pointed out previously, due to a Fe-As(p_z)-H-As(p_z)-Fe hopping path enabled by the hydrogen $1s$ orbital that is much less strongly bound than the corresponding $2p$ orbitals in the F compound.

This peculiar band introduces an additional Fermi surface of three-dimension character and ellipsoidal shape, something not appearing in other 1111 compounds including the isovalent F compound. Both compounds show very strong Fermi surface nesting at the expected (π,π,0) wave vector. The cylindrical Fermi surfaces are different for the two compounds: circular for the F compound but two surfaces with different radii; not so circular for the H compound but nearly identical surfaces. The unusual band and extra Fermi surface has been discussed, briefly, in terms of the effect of an incipient band that could

help to resolve the differences observed between these two compounds. The differences in orbital occupations in both the Fe and As atomic spheres in the H and F compounds has been quantified. It may be helpful in the future to compare these isovalent substations with the results on H doping of the 1111 class, as in $LaFeAsO_{1-x}H_x$ [38] and $SmFeAsO_{1-x}H_x$ [10].

The effects of indirect electronic doping (La for Ca) and direct doping (Co for Fe) have been contrasted. The effect on the density and character of states near the Fermi level is substantial, so differences in properties, including T_c, are expected. Differences in the nesting of these two electron-doped phases have been described as well. However, with no material-specific theory of T_c in Fe-based superconductors, it would be speculation to try to identify the most important distinctions.

We expect that these several findings will contribute to investigations into the determination of what aspects of these differences are relevant to understand their superconducting distinctions. The observation of a lack of superconducting dome in the phase diagrams of both types of doping, taken at face value, indicates an indifference of superconductivity to details of the electronic structure that is difficult to comprehend, since many studies in Fe-based superconductors point to important effects due to small differences.

ACKNOWLEDGMENTS

We acknowledge useful discussions with X. H. Chen on their experimental data, and helpful comments from X. L. Yu, W. C. Bao, A. S. Botana, and S. Gangopadhyay. This work was supported by NSFC of China under Grants No. 11274310, No. 11474287, and No. 11574315. The calculations were performed at the Center for Computational Science of CASHIPS, the ScGrid of Supercomputing Center and Computer Network Information Center of Chinese Academy of Science. W.E.P. was supported by U.S. National Science Foundation consecutive Grants No. DMR-1207622 and No. DMR-1607139.

[1] M. Rotter, M. Tegel, and D. Johrendt, Superconductivity at 38 K in the Iron Arsenide $(Ba_{1-x}K_x)Fe_2As_2$, Phys. Rev. Lett. **101**, 107006 (2008).

[2] C. G. Fu, Z. Li, G. Li, W. Z. Hu, J. Dong, J. Zhou, X. D. Zhang, P. Zheng, N. L. Wang, and J. L. Luo, Superconductivity in hole-doped $(Sr_{1-x}K_x)Fe_2As_2$, Chin. Phys. Lett. **25**, 3403 (2008).

[3] G. Wu, H. Chen, T. Wu, Y. L. Xie, Y. J. Yan, R. H. Liu, X. F. Wang, J. J. Ying, and X. H. Chen, Different resistivity response to spin-density wave and superconductivity at 20 K in $Ca_{1-x}Na_xFe_2As_2$, J. Phys.: Condens. Matter **20**, 422201 (2008).

[4] X. Y. Zhu, F. Han, G. Mu, P. Cheng, B. Shen, B. Zeng, and H. Wen, Superconductivity in Ti-doped iron-arsenide compound $Sr_4Cr_{0.8}Ti_{1.2}O_6Fe_2As_2$, Sci. China Ser. G **52**, 1876 (2009).

[5] G. F. Chen, T. L. Xia, H. X. Yang, J. Q. Li, P. Zheng, J. L. Luo, and N. L. Wang, Possible high temperature superconductivity in a Ti-doped A-Sc-Fe-As-O (A = Ca, Sr) system, Supercond. Sci. Technol. **22**, 072001 (2009).

[6] Y. Muraba, S. Matsuishi, and H. Hosono, La-substituted CaFeAsH superconductor with $T_c = 47$ K, J. Phys. Soc. Jpn. **83**, 033705 (2014).

[7] Y. Muraba, S. Matsuishi, and H. Hosono, Enhancing the three-dimensional electronic structure in 1111-type iron arsenide superconductors by H substitution?, Phys. Rev. B **89**, 094501 (2014).

[8] T. Hanna, Y. Muraba, S. Matsuishi and H. Hosono, Superconductivity in 1111-type $CaFeAsF_{1-x}H_x$ induced by selective hydrogen elimination, Appl. Phys. Lett. **103**, 142601 (2013).

[9] T. Hanna, Y. Muraba, S. Matsuishi, N. Igawa, K. Kodama, S. Shamoto, and H. Hosono, Hydrogen in layered iron arsenides: Indirect electron doping to induce superconductivity, Phys. Rev. B **84**, 024521 (2011).

[10] H. Takahashi, T. Tomita, H. Soeda, M. Ebata, K. Okuma, T. Hanna, Y. Muraba, S. Matsuishi, and H. Hosono, High-pressure studies for hydrogen substituted $CaFeAsF_{1-x}H_x$ and $SmFeAsO_{1-x}H_x$, J. Supercond. Nov. Magn. **25**, 1293 (2012).

[11] J. Ferber, K. Foyevtsova, R. Valenti, and H. O. Jeschke, LDA + DMFT study of the effects of correlation in LiFeAs, Phys. Rev. B **85**, 094505 (2012).

[12] D. R. Parker, M. J. Pitcher, P. J Baker, I. Franke, T. Lancaster, S. J. Blundell, and S. J. Clarke, Structure, antiferromagnetism and superconductivity of the layered iron arsenide NaFeAs, Chem. Commun. **2009**, 2189 (2009).

[13] H. O. Jeschke, I. I. Mazin, and R. Valentí, Why MgFeGe is not a superconductor, Phys. Rev. B **87**, 241105(R) (2013).

[14] H. B. Rhee and W. E. Pickett, Contrast of LiFeAs with isostructural, isoelectronic, and non-superconducting MgFeGe, J. Phys. Soc. Jpn. **82**, 034714 (2013).

[15] K. Okuma, M. Ebata, T. Tomita, H. Takahashi, T. Hanna, Y. Muraba, S. Matsuishi, and H. Hosono, High-pressure studies for hydrogen substituted $CaFeAsF_{1-x}H_x$, J. Phys.: Conf. Ser. **400**, 022092 (2012).

[16] P. Cheng, Z. J. Xiang, G. J. Ye, X. F. Lu, B. Lei, A. F. Wang, F. Chen, and X. G. Luo, Transport properties and electronic phase diagram of cobalt-doped 1111-type iron arsenide hydride, Supercond. Sci. Technol. **27**, 065012 (2014).

[17] Y. Taguchi, A. Kitora, and Y. Isawa, Increase in T_c upon Reduction of Doping in Li_xZrNCl Superconductors, Phys. Rev. Lett. **97**, 107001 (2006).

[18] A. S. Botana and W. E. Pickett, Dielectric response of electron-doped ionic superconductor Li_xZrNCl, Phys. Rev. B **90**, 125145 (2014).

[19] G. Wang, X. B. Shi, H. P. Liu, and Q. B. Liu, Electronic structures and magnetism of CaFeAsH and CaFeAsF, J. Phys. Soc. Jpn. **84**, 054708 (2015).

[20] X. Chen, S. Maiti, A. Linscheid, and P. J. Hirschfeld, Electron pairing in the presence of incipient bands in iron-based superconductors, Phys. Rev. B **92**, 224514 (2015).

[21] Y. Kamihara, T. Watanabe, M. Hirano, and H. Hosono, Iron-based layered superconductor $La[O_{1-x}F_x]FeAs$ ($x = 0.05$–0.12) with $T_c = 26$ K, J. Am. Chem. Soc. **130**, 3296 (2008).

[22] H. Okada, H. Takahashi, S. Y. Matsuishi, M. Hirano, H. Hosono, K. Matsubayashi, Y. Uwatoko, and H. Takahashi, Pressure dependence of the superconductor transition temperature of $Ca(Fe_{1-x}Co_x)AsF$ compounds: A comparison with the effect of pressure on $LaFeAsO_{1-x}F_x$, Phys. Rev. B **81**, 054507 (2010).

[23] S. K. Mishra, R. Mittal, S. L. Chaplot, S. V. Ovsyannikov, D. M. Trots, L. Dubrovinsky, Y. Su, Th. Brueckel, S. Matuishi, H. Hosono, and G. Garbarino, Pressure dependence of the low-temperature crystal structure and phase transition behavior of CaFeAsF and SrFeAsF: A synchrotron x-ray diffraction study, Phys. Rev. B **84**, 224513 (2011).

[24] S. Matsuishi, Y. Inoue, T. Nomura, Y. Kamihara, M. Hirano, and H. Hosono, Effect of 3*d* transition metal doping on the superconductivity in quaternary fluoroarsenide CaFeAsF, New J. Phys. **11**, 025012 (2009).

[25] P. Blaha, K. Schwarz, G. K. H. Madsen, D. Kvasnicka, and J. Luitz. *WIEN2K, An Augmented Plane Wave + Local Orbitals Program for Calculating Crystal Properties* (Karlheinz Schwarz, Techn, Universität Wien, Austria 2001).

[26] J. P. Perdew, K. Burke, and M. Ernzerhof, Generalized Gradient Approximation Made Simple, Phys. Rev. Lett. **77**, 3865 (1996).

[27] S. Lebegue, Z. P. Yin, and W. E. Pickett, The delicate electronic and magnetic structure of the LaFePnO system (Pn = pnictogen), New J. Phys. **11**, 025004 (2009).

[28] J. C. Smith, S. Banerjee, V. Pardo, and W. E. Pickett, Dirac Point Degenerate with Massive Bands at a Topological Quantum Critical Point, Phys. Rev. Lett. **106**, 056401 (2011).

[29] V. Pardo, J. C. Smith, and W. E. Pickett, Linear Bands, Zero-momentum Weyl semimetals, and topological transition in skutterudite-structure pnictides, Phys. Rev. B **85**, 214531 (2012).

[30] Y.-Z. Zhang, I. Opahle, H. O. Jeschke, and R. Valenti, Itinerant nature of magnetism in iron pnictides: A first-principles study, Phys. Rev. B **81**, 094505 (2010).

[31] D. Y. Liu, Y. M. Quan, Z. Zeng, and L. J. Zou, A three-dimensional tight-binding model and magnetic instability of iron selenide KFe_2Se_2, Physica B **407**, 1139 (2012).

[32] W. E. Pickett, J. M. An, H. Rosner, and S. Y. Savrasov, Role of two dimensionality in MgB_2, Physica C **387**, 117 (2003).

[33] W. E. Pickett, Electron-phonon coupling in MgB_2-like materials: Its magnitude and its limits, Braz. J. Phys. **33**, 695 (2003).

[34] L. Ortenzi, H. Gretarsson, S. Kasahara, Y. Matsuda, T. Shibauchi, K. D. Finkelstein, W. Wu, S. R. Julian, Y.-J. Kim, I. I. Mazin, and L. Boeri, Structural Origin of the Anomalous Temperature Dependence of the Local Magnetic Moments in the $CaFe_2As_2$ Family of Materials, Phys. Rev. Lett. **114**, 047001 (2015).

[35] M. J. Han, Q. Yin, W. E. Pickett, and S. Y. Savrasov, Anisotropy, Itineracy, and Magnetic Frustration in High T_c Iron Pnictides, Phys. Rev. Lett. **102**, 107003 (2009).

[36] Y.-N. Huang, X.-L. Yu, D.-Y. Liu, and L.-J. Zou, Magnetism and electronic structures of novel layered $CaFeAs_2$ and $Ca_{0.75}(Pr/La)_{0.25}FeAs_2$, J. Appl. Phys. **117**, 17E113 (2015).

[37] D. Y. Liu, Y. M. Quan, D. M. Chen, L. J. Zou, and H. Q. Lin, Ferro-orbital order induced by electron-lattice coupling in orthorhombic iron pnictides, Phys. Rev. B **84**, 064435 (2011).

[38] S. Iimura, S. Matsuishi, H. Sato, T. Hanna, Y. Muraba, S. W. Kim, J. E. Kim, M. Takata, and H. Hosono, Two-dome structure in electron-doped iron arsenide superconductors, Nat. Commun. **3**, 943 (2013).